IOPscience iopscience.iop.org

Home Search Collections Journals About Contact us My IOPscience

Mutual impedance of air-cored coils above a conducting plate

This article has been downloaded from IOPscience. Please scroll down to see the full text article.

2004 J. Phys. D: Appl. Phys. 37 1857

(http://iopscience.iop.org/0022-3727/37/13/021)

View the table of contents for this issue, or go to the journal homepage for more

Download details:
IP Address: 35.8.11.2
The article was downloaded on 02/07/2013 at 18:31

Please note that terms and conditions apply.

INSTITUTE OF PHYSICS PUBLISHING JOURNAL OF PHYSICS D: APPLIED PHYSICS

J. Phys. D: Appl. Phys. **37** (2004) 1857–1868 PII: S0022-3727(04)75906-9

# Mutual impedance of air-cored coils above a conducting plate

**S K Burke**[1] **and M E Ibrahim**[1,2]

[1] Defence Science and Technology Organisation, 506 Lorimer St, Fishermans Bend VIC 3207, Australia

[2] School of Physics and Materials Engineering, Monash University, Wellington Rd, Clayton VIC 3800, Australia

Received 6 February 2004
Published 16 June 2004
Online at stacks.iop.org/JPhysD/37/1857
doi:10.1088/0022-3727/37/13/021

**Abstract**

The change in mutual impedance $\Delta Z_{12}$ due to eddy-current induction is considered for an arbitrary pair of air-cored coils located above a conducting plate. A general expression is derived for $\Delta Z_{12}$ and applied to the specific case of cylindrical coils with rectangular cross-section. A series of closed-form expressions for $\Delta Z_{12}$ is presented for the geometries that cover all of the possible coil configurations for which the orientation of the individual coils is either normal or tangential to the plate. Expressions are also obtained for $\Delta Z_{12}$ in the dipole limit and the results are compared with earlier work for dipole loops. The validity of the theory is tested against experimental measurements for representative high-symmetry coil systems above an aluminium-alloy plate. The theoretical calculations and experimental results are in excellent agreement over the experimental frequency range 100 Hz–50 kHz. The significance of the results for eddy-current non-destructive inspection using driver–pickup coils is discussed.

## 1. Introduction

Eddy-current non-destructive inspection (NDI) is used in the aerospace, energy and manufacturing industries to detect structural defects such as cracks and hidden corrosion in critical metal components. In this technique, eddy currents are induced in the component using a probe-coil carrying an alternating current. The presence of a defect that perturbs the eddy-current distribution is then detected via the resulting change in the induced coil voltage or coil impedance. In the simplest case, the same coil acts as both a transmitter and receiver, often in conjunction with a second coil used as a reference impedance for differential measurements. In more sophisticated applications, separate transmitter ('driver') and receiver ('pickup') coils are employed to exploit the additional sensitivity and flexibility which can be obtained by optimizing the individual transmitter and receiver functions.

The response of driver–pickup coil systems is dictated by the change in mutual impedance due to the defect, and the coil configuration is designed to minimize the effects of coil liftoff, temperature fluctuations and other sources of unwanted signals while maximizing the defect response. Practical applications of driver–pickup coil arrangements include axisymmetric reflection probes for measurement of conductivity and coating thickness (Deeds *et al* 1979), through-transmission systems for characterization of metallic sheets (Dodd and Deeds 1982), circular-driver/differential-pickup coils for surface crack detection (Auld *et al* 1989), remote-field eddy-current systems for pipe inspection (Schmidt 1989, Haugland 1996) and sliding coils for detection and sizing of cracks in lap joints and heat-exchanger tubing (Mayos and Muller 1987, Cecco *et al* 1993, Obrutsky *et al* 1996). More complex configurations, which rely on orthogonal driver–pickup coils, have also been proposed for detecting and sizing defects in other specialized applications (Beissner and Sablik 1984, Popa *et al* 1997, Grimberg *et al* 2000, Hoshikawa *et al* 2001).

While there is a large choice of theoretical models to predict the response for single coil systems, and the general theoretical framework for predicting the response of driver–pickup systems is well developed (Auld and Moulder 1999), there are few analytical treatments in the literature for driver–pickup systems in eddy-current NDI. In much of the work cited above, either semi-empirical or finite-element analysis rather than analytical methods have been used

 © 2004 IOP Publishing Ltd Printed in the UK 

to predict the system response and optimize the inspection parameters. Closed-form analytical expressions have been derived to predict the response for axisymmetric driver–pickup geometries including coaxial coils above a layered half-space, coaxial through-transmission systems and transmit–receive coils in boreholes (Dodd *et al* 1971, Dodd and Deeds 1982, Dodd *et al* 1974). Moving beyond axisymmetric geometries, closed-form expressions for the mutual impedance of dipole transmit–receive coils above a half-space are available in the geophysics literature for a variety of coil orientations (Wait 1982, Zhang *et al* 2000). However, in geophysics applications, the coil separation is usually sufficiently large that the transmitter and receiver coils can be treated as dipole sources. This approximation is of limited usefulness in eddy-current NDI because the driver and pickup coils are in close proximity.

The aim of this work is to examine the change in mutual impedance $\Delta Z_{12}$ due to eddy-current induction for finite-size air-cored driver–pickup coils above a defect-free conducting plate. In section 2, a general expression is derived for $\Delta Z_{12}$ and applied to the canonical case of cylindrical coils with rectangular cross-section. A series of closed-form expressions for $\Delta Z_{12}$ is then presented for all of the possible coil configurations in which the orientation of the individual coils is either normal or tangential to the plate. Expressions are also obtained for $\Delta Z_{12}$ in the dipole limit and the results compared with earlier work for dipole loops. The validity of the theory is tested against experimental measurements for representative high-symmetry coil systems above an aluminium-alloy plate in section 4. Finally, the significance of the results for eddy-current NDI using driver–pickup coils is discussed in section 5.

## 2. Theory

The problem is shown schematically in figure 1, where a pair of air-cored coils forming a driver–pickup system is placed above an infinite conducting plate. The shape and orientation of the coils is arbitrary, and the minimum distance between the surface of the plate and the coil windings is denoted by $z_{0d}$ and $z_{0p}$ for the driver and pickup coils, respectively. The driver coil is driven by an alternating current of the form $I\exp(\mathrm{i}\omega t)$ and the voltage $V$ induced in the pickup coil consists of a response due to direct coupling with the driver coil together with a response due to induced currents and magnetization in the plate. The plate is uniform and isotropic with thickness $c$, electrical resistivity $\rho$ and (constant) relative magnetic permeability $\mu_r$. As is usual in eddy-current induction problems, the frequency is assumed to be sufficiently low (i.e. $<10$ MHz) that the displacement current can be neglected and the quasi-static approximation can be used. The fields are assumed to have reached a steady state sinusoidal time dependence of the form $\exp(\mathrm{i}\omega t)$ and phasor notation will be used.

The change in the mutual (or transfer) impedance $\Delta Z_{12}$ due to the plate is defined as the difference in mutual impedance when the coil system is above the plate and in the absence of the plate. For ideal coils and ideal voltage measurements (infinite input impedance), $Z_{12} = V/I = \mathrm{i}\omega M$, where $M$ is the mutual inductance. There are two possible methods for calculating $\Delta Z_{12}$. The first method is to: (i) compute the magnetic field produced by the current density induced in the plate by the driver coil; (ii) integrate over the pickup coil to determine the resulting contribution to the magnetic flux $\Delta\Phi$ and (iii) form $\Delta Z_{12} = \mathrm{i}\omega\Delta\Phi/I$. The second approach is to use the two-port $\Delta Z$ formula derived from the Lorentz reciprocity relations by Auld and Moulder (1999) and reduce the problem to the evaluation of an integral over the surface of the plate. The latter approach, developed below, will be used here.

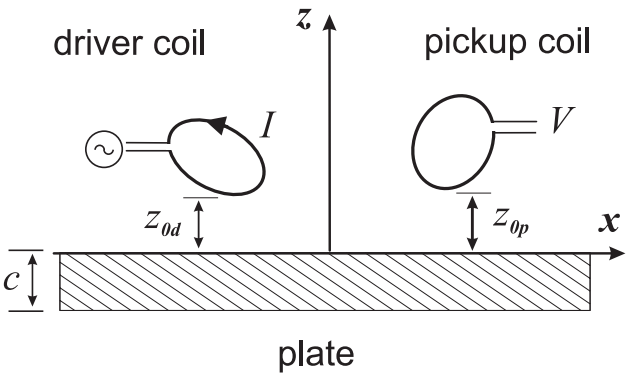


**Figure 1.** Air-cored driver–pickup coil system above an isotropic conducting plate.

### 2.1. Change in mutual impedance due to an infinite conducting plate

From Auld and Moulder (1999), the change in the mutual impedance due to the plate is given by the surface integral

$$\Delta Z_{12} = \frac{1}{I^2}\iint_{S_F} (\boldsymbol{E}_a \times \boldsymbol{H}_b - \boldsymbol{E}_b \times \boldsymbol{H}_a)\cdot\hat{\boldsymbol{n}}\,\mathrm{d}S, \qquad (1)$$

where the subscript a refers to the fields generated by the driver coil in the absence of the plate, b denotes the fields generated by the pickup coil acting as a driver in the presence of the plate, $S_F$ is an arbitrary closed surface bounding the plate (but excluding the coils), $\hat{\boldsymbol{n}}$ is the unit outward normal to $S_F$ and $I$ is the amplitude of the driving current.

For the plate geometry considered in this paper, $S_F$ is chosen to be $\{z = 0^+\}$-the plane an infinitesimal distance above the top surface of the plate and $S_\infty$-the hemispherical surface shown in figure 2. In the limit $R \to \infty$, the contribution to the surface integral arising from $S_\infty$ tends to zero and equation (1) can be written as an integral over $\{z = 0^+\}$

$$\Delta Z_{12} = \frac{1}{I^2}\iint_{\{z=0^+\}} (\boldsymbol{E}_a \times \boldsymbol{H}_b - \boldsymbol{E}_b \times \boldsymbol{H}_a)\cdot\hat{\boldsymbol{z}}\,\mathrm{d}S. \qquad (2)$$

As the plane $z = 0^+$ is a current-free region, equation (2) can be simplified by representing the magnetic field in terms of a magnetic scalar potential $\phi$

$$\boldsymbol{H} = I\nabla\phi. \qquad (3)$$

Substituting for the magnetic fields in equation (2) using equation (3), then integrating by parts (Beissner 1988), the change in mutual impedance becomes

$$\Delta Z_{12} = \mathrm{i}\omega\mu_0 \int\int_{\{z=0^+\}} \left(\phi_d^{(s)}\frac{\partial\phi_p}{\partial z} - \phi_p\frac{\partial\phi_d^{(s)}}{\partial z}\right)\mathrm{d}x\,\mathrm{d}y, \qquad (4)$$

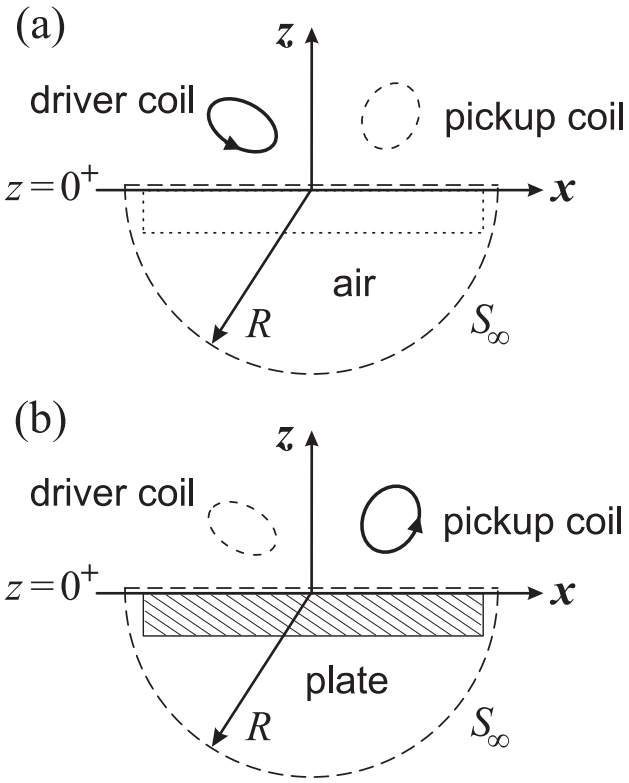


**Figure 2.** Driver and pickup coils above a conducting plate showing the configurations required for computation of $\Delta Z_{12}$ according to equation (1): (*a*) driver coil in free space and (*b*) pickup coil acting as a driver coil above the plate.

where $\phi_{\mathrm{d}}^{(\mathrm{s})}$ is the magnetic scalar potential for the driver coil in the absence of the plate (figure 2(*a*)) and $\phi_{\mathrm{p}}$ is the magnetic scalar potential in the case where the pickup coil acts as a driver coil in the presence of the plate (figure 2(*b*)). In the following, it is assumed that the incident or 'source' fields, i.e. the fields due to the coils in the absence of the plate, are known (e.g. from the Biot–Savart law or otherwise, Hannakam 1972, Theodoulidis and Kriezis 2002) and hence $\phi_{\mathrm{d}}^{(\mathrm{s})}$ is considered to be a known quantity.

To proceed further it is necessary to obtain an expression for $\phi_{\mathrm{p}}$. From previous work (e.g. Burke (1990)), it can be shown that the magnetic scalar potential for an arbitrary coil above a conducting plate can be expressed in terms of the two-dimensional Fourier transform of the source magnetic scalar potential incident on the surface of the plate $z = 0$, so that for $0 \leqslant z \leqslant z_{0\mathrm{p}}$

$$\tilde{\phi}_{\mathrm{p}}(u, v; z) = \tilde{\phi}_{\mathrm{p}}^{(\mathrm{s})}(u, v; z = 0)[\exp(\alpha z) - \exp(-\alpha z)R(\alpha)], \tag{5}$$

where the superscript (s) indicates a 'source' parameter, the tilde denotes the two-dimensional Fourier transform

$$\tilde{g}(u, v; z) = \frac{1}{2\pi}\int_{-\infty}^{+\infty}\int_{-\infty}^{+\infty} \exp(-\mathrm{i}ux - \mathrm{i}vy) \times g(x, y, z)\,\mathrm{d}x\,\mathrm{d}y, \tag{6}$$

$\alpha^2 = u^2 + v^2$ and $\phi_{\mathrm{p}}^{(\mathrm{s})}$ is the (known) incident scalar potential due to the pickup coil source. In equation (5) $R(\alpha)$ is the 'reflection coefficient' for the plate

$$R(\alpha) = \frac{(\mu_{\mathrm{r}}\alpha - \alpha_1)(\mu_{\mathrm{r}}\alpha + \alpha_1)[1 - \exp(-2\alpha_1 c)]}{(\mu_{\mathrm{r}}\alpha + \alpha_1)^2 - (\mu_{\mathrm{r}}\alpha - \alpha_1)^2\exp(-2\alpha_1 c)}, \tag{7}$$

where $\alpha_1 = \sqrt{\alpha^2 + 2\mathrm{i}/\delta^2}$ and $\delta = \sqrt{2\rho/(\omega\mu_0\mu_{\mathrm{r}})}$ is the electromagnetic skin depth. The two-dimensional Fourier transform of the incident magnetic scalar potential for a driver coil source can be written in a similar fashion so that, for $0 \leqslant z \leqslant z_{0\mathrm{d}}$,

$$\tilde{\phi}_{\mathrm{d}}(u, v; z) = \tilde{\phi}_{\mathrm{d}}^{(\mathrm{s})}(u, v; z = 0)\exp(\alpha z). \tag{8}$$

Substituting for $\phi_{\mathrm{d}}^{(\mathrm{s})}$ and $\phi_{\mathrm{p}}$ in equation (4) using the Fourier transforms (5) and (8), applying the Parseval theorem and noting that $\hat{z}\cdot\tilde{\boldsymbol{H}}^{(\mathrm{s})}(u, v; z) = \alpha\tilde{\phi}^{(\mathrm{s})}(u, v; z)$, the change in mutual impedance due to the plate reduces to the final form

$$\Delta Z_{12} = 2\mathrm{i}\omega\mu_0\int_{-\infty}^{+\infty}\int_{-\infty}^{+\infty}\frac{1}{\alpha}\tilde{h}_{\mathrm{p}}^{*(\mathrm{s})}\tilde{h}_{\mathrm{d}}^{(\mathrm{s})}R(\alpha)\,\mathrm{d}u\,\mathrm{d}v, \tag{9}$$

where the 'source functions' for the driver and pickup coils

$$\tilde{h}_{\mathrm{d}}^{(\mathrm{s})} = \frac{\tilde{H}_{z\mathrm{d}}^{(\mathrm{s})}(u, v; z = 0)}{I}$$
$$\tilde{h}_{\mathrm{p}}^{*(\mathrm{s})} = \frac{\tilde{H}_{z\mathrm{p}}^{(\mathrm{s})}(-u, -v; z = 0)}{I} \tag{10}$$

are related to the respective two-dimensional Fourier transforms of the normal component of the free-space magnetic field incident on the top surface of the plate due to (i) the driver coil (driven by unit current) and (ii) the pickup coil (driven by unit current). Thus, the evaluation of the mutual impedance for air-cored driver and pickup coils of arbitrary geometry is reduced to the evaluation of the double integral (9) involving the known source functions (10).

The expression (9) is valid for an air-cored coil system with arbitrary shape and orientation above an infinite conducting plate. In this paper, we will consider cylindrical air-cored coils, the most common type of coil construction, and treat all possible coil configurations for which the orientation of the individual coils is either normal or tangential to the surface of the plate. The driver coil consists of $N_{\mathrm{d}}$ turns, inner radius $a_{1\mathrm{d}}$, outer radius $a_{2\mathrm{d}}$ and winding thickness $2t_{\mathrm{d}}$ while the pickup coil has $N_{\mathrm{p}}$ turns, inner radius $a_{1\mathrm{p}}$, outer radius $a_{2\mathrm{p}}$ and winding thickness $2t_{\mathrm{p}}$. The centroids of the driver and pickup coils are located at heights $z_{\mathrm{d}}$ and $z_{\mathrm{p}}$, respectively, above the surface of the plate and the coil centres are separated by a horizontal distance $d \geqslant 0$. For convenience, the coil centred at the origin is assumed to be the driver coil, but in line with the reciprocity theorem, the mutual impedance is independent of which coil is actually acting as the driver coil.

There are three general cases: (i) both coils have their axes normal to the surface of the plate ('pancake coils'), (ii) both coils have their axes tangential to the surface ('tangent coils') and (iii) the axis of one coil is normal to the surface and the other is tangential ('pancake–tangent coils'). Within this broad classification, there are six distinct high-symmetry coil configurations. These systems are depicted in figure 3, where the notation for Systems I–IV correspond to that in Wait's treatment of dipole loops (Wait 1982). In System I, the axes of both coils are normal to the surface of the plate, and incorporates the familiar reflection coil geometry when the coils are coaxial, $d = 0$, and the sliding probe geometry

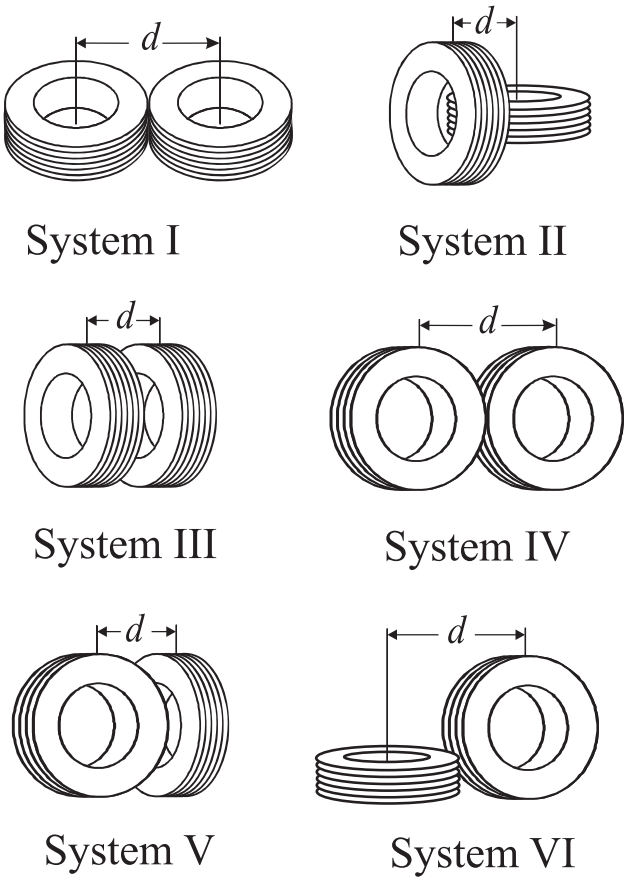


**Figure 3.** The six high-symmetry configurations for cylindrical driver–pickup coils on a conducting plate (schematic). The notation follows that of Wait (1982) for dipole loops.

when the coils are displaced, $d > a_{2p} + a_{2d}$. In System II, the axis of the driver coil is normal to the surface, the axis of the pickup coil is tangent to the surface and the axes are coplanar. In the special case when the coil centres are at the same height ($z_p = z_d$) the inductive coupling between the coils is zero in the absence of the plate. Systems III and IV are in fact special cases of the parallel tangent coil geometry where the axes of the coils are tangential to the surface of the plate and parallel to each other. There is no inductive coupling between the coils in Systems V and VI, which are special high-symmetry cases of the more general tangent–tangent and pancake–tangent coil configurations, respectively. Transmission geometries, where the driver and pickup coils are situated on opposite sides of the plate, are not considered here.

In the following sections, exact closed-form expressions for $\Delta Z_{12}$ for the possible driver–pickup coil configurations will be derived by substituting the appropriate expressions for the source functions into the general expression (9) and evaluating the resulting surface integral. Pancake coil systems are considered in section 2.2, pancake–tangent coil systems are considered in section 2.3, and tangent coil configurations are treated in sections 2.4 and 2.5. The validity of the resulting expressions is tested by taking the limit for small coil dimensions and comparing the results for the high-symmetry systems with the corresponding expressions obtained by Wait (1982) for dipole loops above a half-space.

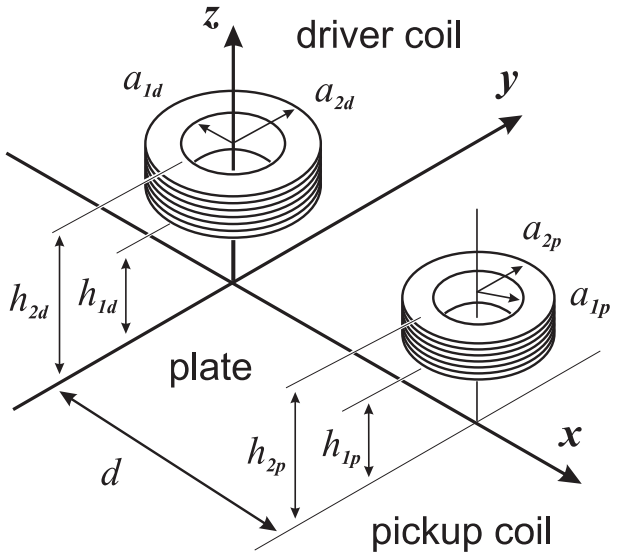


**Figure 4.** System I. Schematic diagram showing the pancake coil configuration.

### 2.2. System I: pancake coils

In this geometry, shown schematically in figure 4, the axes of both the driver coil and the pickup coil are normal to the surface of the plate and the axes of the coils are separated by a distance $d \geqslant 0$ along the $x$-axis. The source fields for this geometry are well known (Dodd and Deeds 1968) and the normal component of the incident magnetic field on the surface of the plate $z = 0$ due to the pickup coil can be written as the integral,

$$H_{zp}^{(s)} = \frac{1}{2} n_p I \int_0^\infty \frac{1}{\alpha^2} J(\alpha a_{1p}, \alpha a_{2p}) \times [\exp(-\alpha h_{1p}) - \exp(-\alpha h_{2p})] J_0(\alpha\sqrt{(x-d)^2 + y^2})\, d\alpha, \tag{11}$$

where $h_{1p}$ is the height of the bottom of the windings above the surface of the plate, $h_{2p}$ is the height of the top of the windings above the plate, $n_p$ is the turn density of the pickup coil, $n_p = N_p/[(a_{2p} - a_{1p})(h_{2p} - h_{1p})]$, and $J(\alpha a_{1d}, \alpha a_{2d})$ denotes the radial integral

$$\begin{aligned} J(x_1, x_2) &= \int_{x_1}^{x_2} x J_1(x)\, dx \\ &= \frac{\pi}{2}[x_1\{J_0(x_1)\boldsymbol{H}_1(x_1) - J_1(x_1)\boldsymbol{H}_0(x_1)\} \\ &\quad - x_2\{J_0(x_2)\boldsymbol{H}_1(x_2) - J_1(x_2)\boldsymbol{H}_0(x_2)\}], \end{aligned} \tag{12}$$

where $J_n$ are Bessel functions of the first kind of order $n$ and the $\boldsymbol{H}_n$ are Struve functions of order $n$. Adapting the expression for the pickup coil source field (11) to the driver coil case, the normal component of the incident magnetic field on the surface of the plate due to the driver coil is

$$H_{zd}^{(s)} = \frac{1}{2} n_d I \int_0^\infty \frac{1}{\alpha^2} J(\alpha a_{1d}, \alpha a_{2d}) \times [\exp(-\alpha h_{1d}) - \exp(-\alpha h_{2d})] J_0(\alpha\sqrt{x^2 + y^2})\, d\alpha, \tag{13}$$

where the subscript d is used to denote the corresponding driver coil parameters. The required two-dimensional Fourier transforms of the incident fields on the surface of the plate, equations (11) and (13), can be obtained using the results of

the appendix,

$$\tilde{h}_{\mathrm{p}}^{*(\mathrm{s})} = \frac{n_{\mathrm{p}}}{2\alpha^3}\exp(\mathrm{i}ud)J(\alpha a_{1\mathrm{p}}, \alpha a_{2\mathrm{p}}) \times [\exp(-\alpha h_{1\mathrm{p}}) - \exp(-\alpha h_{2\mathrm{p}})], \tag{14}$$

$$\tilde{h}_{\mathrm{d}}^{(\mathrm{s})} = \frac{n_{\mathrm{d}}}{2\alpha^3}J(\alpha a_{1\mathrm{d}}, \alpha a_{2\mathrm{d}})[\exp(-\alpha h_{1\mathrm{d}}) - \exp(-\alpha h_{2\mathrm{d}})]. \tag{15}$$

Substituting the source fields (14) and (15) into the general expression (9) and changing variables to cylindrical coordinates ($u = \alpha\cos\varphi$, $v = \alpha\sin\varphi$)

$$\Delta Z_{12} = \frac{1}{2}\mathrm{i}\omega\mu_0 n_{\mathrm{d}} n_{\mathrm{p}} \int_0^\infty \frac{\mathrm{d}\alpha}{\alpha^6} J(\alpha a_{1\mathrm{d}}, \alpha a_{2\mathrm{d}}) J(\alpha a_{1\mathrm{p}}, \alpha a_{2\mathrm{p}}) \times[\exp(-\alpha h_{1\mathrm{d}}) - \exp(-\alpha h_{2\mathrm{d}})] \times[\exp(-\alpha h_{1\mathrm{p}}) - \exp(-\alpha h_{2\mathrm{p}})]R(\alpha) \times \int_0^{2\pi} \mathrm{d}\varphi \exp(\mathrm{i}\alpha d\cos\varphi). \tag{16}$$

The integral over $\varphi$ is simply $2\pi J_0(\alpha d)$ from the definition of the Bessel function $J_0$ and hence the change in mutual impedance can be written in the final form

$$\Delta Z_{12} = \mathrm{i}\omega\mu_0 n_{\mathrm{d}} n_{\mathrm{p}} \pi \int_0^\infty \frac{1}{\alpha^6} J(\alpha a_{1\mathrm{d}}, \alpha a_{2\mathrm{d}}) J(\alpha a_{1\mathrm{p}}, \alpha a_{2\mathrm{p}}) \times J_0(\alpha d)[\exp(-\alpha h_{1\mathrm{d}}) - \exp(-\alpha h_{2\mathrm{d}})] \times[\exp(-\alpha h_{1\mathrm{p}}) - \exp(-\alpha h_{2\mathrm{p}})]R(\alpha)\,\mathrm{d}\alpha. \tag{17}$$

This closed-form expression is symmetric on interchange of the driver–pickup coil designation and, in the special case where $d = 0$, reproduces the known result for a coaxial reflection coil (Dodd and Deeds 1968).

*2.2.1. Dipole approximation.* The validity of equation (17) can be checked by comparing it with published results derived in the dipole limit. For small coil dimensions, the functions that enter the integrand in equation (17) reduce to the form

$$J(\alpha a_{1\mathrm{p}}, \alpha a_{2\mathrm{p}}) = \frac{\alpha^3(a_{2\mathrm{d}}^3 - a_{1\mathrm{d}}^3)}{6} + \cdots, \tag{18}$$

$$\exp(-\alpha h_{1\mathrm{d}}) - \exp(-\alpha h_{2\mathrm{d}}) = 2\alpha t_{\mathrm{d}}\exp(-\alpha z_{\mathrm{d}}) + \ldots, \tag{19}$$

with similar expressions for the pickup coil functions. In equation (19) $z_{\mathrm{d}} = (h_{1\mathrm{d}} + h_{2\mathrm{d}})/2$ denotes the height of the centre of the driver coil from the surface of the plate and similarly $z_{\mathrm{p}}$ is the height of the centre of the pickup coil above the surface of the plate. Substituting equations (18) and (19) and the similar equations for the pickup coil functions into equation (17) gives the dipole approximation for the mutual impedance in the pancake coil geometry,

$$\Delta Z_{12} = \frac{\mathrm{i}\omega\mu_0 m_{\mathrm{d}} m_{\mathrm{p}}}{4\pi}\int_0^\infty \alpha^2 J_0(\alpha d)\exp[-\alpha(z_{\mathrm{d}} + z_{\mathrm{p}})]R(\alpha)\,\mathrm{d}\alpha \tag{20}$$

where

$$m_{\mathrm{d}} = \frac{\pi N_{\mathrm{d}}(a_{2\mathrm{d}}^2 + a_{2\mathrm{d}}a_{1\mathrm{d}} + a_{1\mathrm{d}}^2)}{3}, \tag{21}$$

is the dipole moment of the driver coil for unit current, with a similar expression for the dipole moment $m_{\mathrm{p}}$ of the pickup coil. This expression is consistent with Wait's half-space result for System I when expressed in terms of the dipole moments of the two current loops, except for an overall sign difference due to a difference in the definition of the isolated coil mutual impedance. While both the dipole expression (20) and the exact result (17) require numerical evaluation of a one-dimensional semi-infinite integral, the dipole approximation offers a slight computational advantage because the integrand does not involve the oscillatory special function $J(x_1, x_2)$.

*2.3. Systems II and VI: pancake–tangent coil geometries*

In this case the axis of the driver coil is again normal to the surface of the plate but the axis of the pickup coil is tangential to the surface and lies at an arbitrary angle $\Theta$ to the horizontal radius drawn between the coil centres. By virtue of the cylindrical symmetry of the driver coil, the pancake–tangent coil geometry can be defined according to figure 5 without loss of generality. Here, the $z$-axis coincides with the driver coil axis, the axis of the pickup coil is parallel to the $x$-axis and the centre of the pickup coil is ($x_{\mathrm{p}} = d\cos\Theta$, $y_{\mathrm{p}} = d\sin\Theta$, $z_{\mathrm{p}}$). System II corresponds to the high-symmetry case where the axes of the two coils are co-planar, $\Theta = 0$, and for the other high-symmetry case, System VI, $\Theta = 90^\circ$.

In order to construct an explicit expression for $\Delta Z_{12}$ according to equation (9), it is only necessary to obtain an expression for the source function for the pickup coil. The source function for the driver coil is known from the analysis in section 2.2. The normal component of the incident magnetic field due to an air-cored tangent coil above a plate can be deduced from the work of Burke (1986), for example, so that on the surface of the plate

$$H_{z\mathrm{p}}^{(\mathrm{s})} = -\frac{2In_{\mathrm{p}}}{\pi}\int_0^\infty\int_0^\infty \frac{1}{s^3}M(sa_{1\mathrm{p}}, sa_{2\mathrm{p}})\sin(st_{\mathrm{p}}) \times \exp(-qz_{\mathrm{p}})\sin[s(x - x_{\mathrm{p}})]\cos[p(y - y_{\mathrm{p}})]\,\mathrm{d}s\,\mathrm{d}p, \tag{22}$$

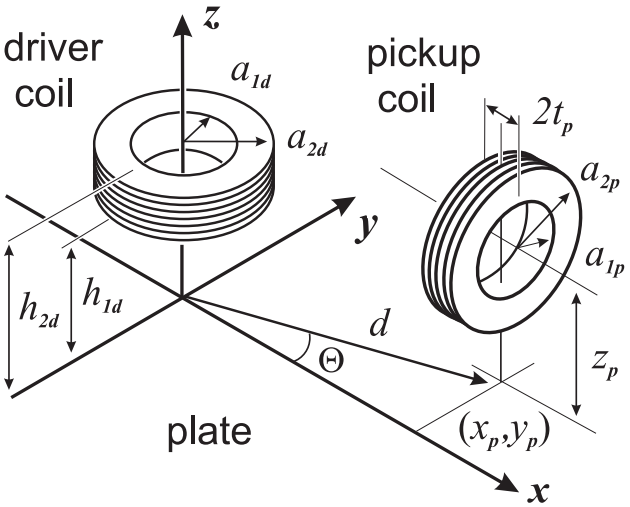


**Figure 5.** Pancake–tangent coil geometry. The coil axes are orthogonal, with the driver coil axis normal to the surface and the pickup coil axis tangent to the surface and parallel to the $x$-axis. There are two special high-symmetry cases: System II, where the coil axes are coplanar, $\Theta = 0$, and System VI where $\Theta = 90^\circ$.

where $q^2 = p^2 + s^2$ and the function $M(sa_{1p}, sa_{2p})$ is defined by the integral

$$M(x_1, x_2) = \int_{x_1}^{x_2} x I_1(x)\,\mathrm{d}x, \tag{23}$$

where $I_n$ is a modified Bessel function of order $n$. $M$ can be represented in terms of known functions as follows

$$M(x_1, x_2) = \frac{\pi}{2}\{x_2[I_1(x_2)\boldsymbol{L}_0(x_2) - I_0(x_2)\boldsymbol{L}_1(x_2)] - x_1[I_1(x_1)\boldsymbol{L}_0(x_1) - I_0(x_1)\boldsymbol{L}_1(x_1)]\}, \tag{24}$$

where $\boldsymbol{L}_n$ denotes the modified Struve function of order $n$. The source function can then be obtained by taking the two-dimensional Fourier transform of the pickup coil incident field (22) (see appendix) to give

$$\tilde{h}_p^{*(s)} = \frac{\tilde{H}_{zp}^{(s)}(-u, -v; 0)}{I} = [-\mathrm{i}n_p \exp(\mathrm{i}ux_p)\exp(\mathrm{i}vy_p) \times \exp(-\alpha z_p)\sin(ut_p)M(ua_{1p}, ua_{2p})]u^{-3}. \tag{25}$$

Substituting for the driver and pickup source functions in equation (9) using equations (15) and (25), the change in mutual impedance due to the plate is given by the double integral

$$\Delta Z_{12} = 4\mathrm{i}\omega\mu_0 n_d n_p \int_0^\infty \int_0^\infty \frac{1}{\alpha^4 u^3}\sin(ut_p)J(\alpha a_{1d}, \alpha a_{2d}) \times M(ua_{1p}, ua_{2p})\exp(-\alpha z_p) \times [\exp(-\alpha h_{1d}) - \exp(-\alpha h_{2d})]\sin(ud\cos\Theta) \times \cos(vd\sin\Theta)R(\alpha)\,\mathrm{d}u\,\mathrm{d}v. \tag{26}$$

In the special case $\Theta = 0$, which corresponds to System II, the real and imaginary parts of $\Delta Z_{12}$ are zero for $d = 0$, vary linearly with $d$ for small $d$ and reach an extremum as $d$ is increased before tending to zero for large $d$. The other high-symmetry configuration (System VI) corresponds to the case $\Theta = 90^\circ$ and the change in mutual impedance is zero for all $d$.

*2.3.1. Dipole approximation.* The change in mutual impedance due to the plate in the dipole limit can be deduced by taking the limit of equation (26) for small coil dimensions. In this limit,

$$M(ua_{1p}, ua_{2p}) = \frac{u^3(a_{2p}^3 - a_{1p}^3)}{6} + \cdots, \tag{27}$$

$$\sin(ut_p)[\exp(-\alpha h_{1d}) - \exp(-\alpha h_{2d})] = 2\alpha u t_p t_d \exp(-\alpha z_d) + \ldots \tag{28}$$

and the limiting form of $J(\alpha a_{1d}, \alpha a_{2d})$ is given by equation (18). Substituting equations (27) and (28) and equation (18) into equation (26) and converting to cylindrical polar coordinates ($u = \alpha\cos\varphi$, $v = \alpha\sin\varphi$)

$$\Delta Z_{12} = \frac{\mathrm{i}\omega\mu_0 m_d m_p}{4\pi} \times \int_0^\infty \alpha^2 \exp[-\alpha(z_d + z_p)]R(\alpha)F_1(\alpha)\,\mathrm{d}\alpha, \tag{29}$$

$$F_1(\alpha) = \frac{2}{\pi}\int_0^{\pi/2} \sin(\alpha d\cos\varphi\cos\Theta)\cos(\alpha d\sin\varphi\sin\Theta) \times \cos\varphi\,\mathrm{d}\varphi, \tag{30}$$

where $m_d$ and $m_p$ are the magnetic dipole moments for the driver and pickup coils, respectively. The angular integral $F_1$ can be evaluated by making some trigonometric simplifications, and noting the definition of the Bessel function $J_1$, to give

$$F_1(\alpha) = \cos\Theta J_1(\alpha d) \tag{31}$$

and hence the change in mutual impedance in the dipole limit reduces to the one-dimensional integral

$$\Delta Z_{12} = \frac{\mathrm{i}\omega\mu_0 m_d m_p}{4\pi}\cos\Theta\int_0^\infty \alpha^2 J_1(\alpha d)\exp[-\alpha(z_d + z_p)] \times R(\alpha)\,\mathrm{d}\alpha, \tag{32}$$

rather than the double integral that appears in the exact expression (26). Equation (32) is again consistent with the result for System II ($\Theta = 0$) derived by Wait (1982) for two dipole loops above a conducting half-space.

### *2.4. Systems III and IV: parallel tangent coil geometries*

The parallel tangent coil geometry is illustrated in figure 6 where two air-cored tangent coils with their axes parallel to each other are located above the plate. The coil axes are parallel to the $x$-axis and the centres of the coils are at positions $(0, 0, z_d)$ and $(x_p, y_p, z_p)$, respectively. This geometry includes, as special cases, the System III geometry for which $y_p = 0$, and System IV for which $x_p = 0$ and the tangent coils are coplanar.

A closed-form expression for $\Delta Z_{12}$ can be derived for the parallel tangent coil geometry following the same approach as in the previous sections. The source function for the tangent pickup coil is again given by equation (25) and, adapting this result, the source function for the tangent driver coil is

$$\tilde{h}_d^{(s)} = \frac{\tilde{H}_{zd}^{(s)}(u, v; z = 0)}{I} = \frac{\mathrm{i}n_d \exp(-\alpha z_d)\sin(ut_d)M(ua_{1d}, ua_{2d})}{u^3}. \tag{33}$$

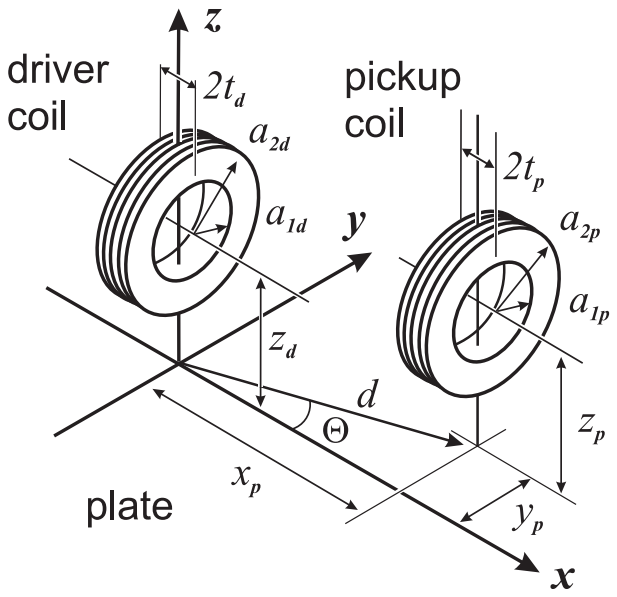


**Figure 6.** Parallel tangent coil geometry. The axes of the coils are parallel to each other and tangential to the surface of the plate. The special cases are (*a*) System III 'double tangent' coils, $\Theta = 0$ and (*b*) System IV 'binocular' or coplanar tangent coils, $\Theta = 90^\circ$.

Substituting equations (25) and (33) into equation (9) and simplifying, the change in mutual impedance due to the plate for the parallel tangent coil geometry can be written in the final form

$$\Delta Z_{12} = 8\mathrm{i}\omega\mu_0 n_\mathrm{d} n_\mathrm{p} \int_0^\infty \int_0^\infty \frac{1}{\alpha u^6} M(ua_{1\mathrm{d}}, ua_{2\mathrm{d}}) \times M(ua_{1\mathrm{p}}, ua_{2\mathrm{p}}) \sin(ut_\mathrm{p}) \sin(ut_\mathrm{d}) \exp[-\alpha(z_\mathrm{p} + z_\mathrm{d})] \times \cos(ud\cos\Theta)\cos(vd\sin\Theta) R(\alpha)\,\mathrm{d}u\,\mathrm{d}v, \quad (34)$$

where the substitutions $x_\mathrm{p} = d\cos\Theta$, $y_\mathrm{p} = d\sin\Theta$ for the pickup coil centre coordinates have been made. As required, equation (34) reduces to the known expression for the change in tangent coil self-impedance in the limit where the driver and pickup coils are identical and $d = 0$ (Clark and Bond 1990). One of the significant features of the parallel tangent coil geometry is the presence of zero-crossings in the real and imaginary parts of the mutual impedance for a given $\Theta$ both as a function of $d$ and frequency. Explicit expressions for the two high-symmetry cases are obtained by substituting $\Theta = 0$ (System III: double tangent coils) and $\Theta = 90^\circ$ (System IV: binocular coils) into the general expression (34).

*2.4.1. Dipole approximation.* The dipole approximation can again be obtained by taking the limit of equation (34) for small coil dimensions. Expanding to first order in coil radius and thickness, and changing the variables of integration from Cartesian coordinates to polar coordinates, equation (34) becomes

$$\Delta Z_{12} = \frac{\mathrm{i}\omega\mu_0 m_\mathrm{d} m_\mathrm{p}}{4\pi} \int_0^\infty \alpha^2 \exp[-\alpha(z_\mathrm{p} + z_\mathrm{d})] R(\alpha) F_2(\alpha)\,\mathrm{d}\alpha, \quad (35)$$

where the angular integral $F_2$ is given by

$$F_2(\alpha) = \frac{2}{\pi}\int_0^{\pi/2} \cos^2\varphi \cos(\alpha d\cos\varphi\cos\Theta) \times \cos(\alpha d\sin\varphi\sin\Theta)\,\mathrm{d}\varphi = \cos^2\Theta J_0(\alpha d) - \frac{\cos 2\Theta J_1(\alpha d)}{\alpha d}. \quad (36)$$

In the special case where $\Theta = 0$ (System III),

$$\Delta Z_{12} = \frac{\mathrm{i}\omega\mu_0 m_\mathrm{d} m_\mathrm{p}}{4\pi} \int_0^\infty \alpha^2 \exp[-\alpha(z_\mathrm{p} + z_\mathrm{d})] \times \left[J_0(\alpha d) - \frac{J_1(\alpha d)}{\alpha d}\right] R(\alpha)\,\mathrm{d}\alpha \quad (37)$$

and for System IV, $\Theta = 90^\circ$,

$$\Delta Z_{12} = \frac{\mathrm{i}\omega\mu_0 m_\mathrm{d} m_\mathrm{p}}{4\pi} \int_0^\infty \alpha^2 \exp[-\alpha(z_\mathrm{p} + z_\mathrm{d})] \times \frac{J_1(\alpha d)}{\alpha d} R(\alpha)\,\mathrm{d}\alpha, \quad (38)$$

again consistent with the expressions derived by Wait (1982) for dipole loops above a half-space.

### 2.5. General tangent coil geometries

The parallel tangent coil geometry considered in section 2.4 is a special case of the more general situation shown schematically in figure 7, where the coil system again consists of tangent coils but where the coil axes are no longer parallel but are oriented at an angle $\chi$ to each other. This general tangent coil geometry includes the high-symmetry configuration System V, where the coil axes are orthogonal, as well as the parallel tangent coil Systems III and IV.

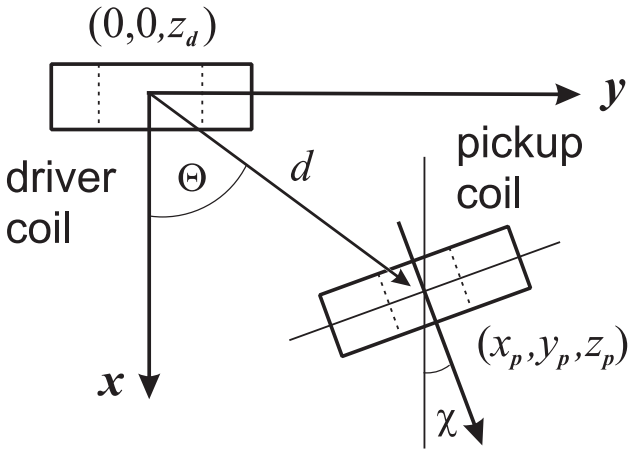


**Figure 7.** General tangent coil geometry (plan view). The driver coil axis is parallel to the $x$-axis and the pickup coil axis is at an arbitrary angle $\chi$ to the driver coil axis. Both coil axes are tangential to the plate.

Consider then a tangent coil system where the centre of the driver coil is at a position $(0, 0, z_\mathrm{d})$ with its axis parallel to the $x$-axis and the pickup coil is located at a position $(x_\mathrm{p}, y_\mathrm{p}, z_\mathrm{p})$ with its axis at an angle $\chi$ with respect to the driver coil axis. The source function for the driver coil is given by equation (33) and the source function for the pickup coil can be found by rotation of equation (25) so that

$$\tilde{h}_\mathrm{p}^{*(\mathrm{s})} = [-\mathrm{i}n_\mathrm{p}\exp(\mathrm{i}ux_\mathrm{p})\exp(\mathrm{i}vy_\mathrm{p})\exp(-\alpha z_\mathrm{p})\sin(u't_\mathrm{p}) \times M(u'a_{1\mathrm{p}}, u'a_{2\mathrm{p}})][u']^{-3}, \quad (39)$$

where

$$u' = u\cos\chi + v\sin\chi = \alpha\cos(\varphi - \chi), \qquad v' = -u\sin\chi + v\cos\chi = \alpha\sin(\varphi - \chi) \quad (40)$$

are the rotated coordinates. Substituting equations (33) and (39) into equation (9) results in the change in mutual impedance

$$\Delta Z_{12} = 2\mathrm{i}\omega\mu_0 n_\mathrm{d} n_\mathrm{p} \int_{-\infty}^\infty \int_\infty^\infty \frac{1}{\alpha u^3 (u')^3} M(ua_{1\mathrm{d}}, ua_{2\mathrm{d}}) \times M(u'a_{1\mathrm{p}}, u'a_{2\mathrm{p}}) \sin(u't_\mathrm{p}) \sin(ut_\mathrm{d}) \exp[-\alpha(z_\mathrm{p} + z_\mathrm{d})] \times \exp(\mathrm{i}ux_\mathrm{p})\exp(\mathrm{i}vy_\mathrm{p}) R(\alpha)\,\mathrm{d}u\,\mathrm{d}v. \quad (41)$$

If the tangent coil axes are orthogonal ('crossed') $\chi = 90^\circ$, equation (41) reduces to the form

$$\Delta Z_{12} = -8\mathrm{i}\omega\mu_0 n_\mathrm{d} n_\mathrm{p} \int_0^\infty \int_0^\infty \frac{1}{\alpha u^3 v^3} M(ua_{1\mathrm{d}}, ua_{2\mathrm{d}}) \times M(va_{1\mathrm{p}}, va_{2\mathrm{p}}) \sin(vt_\mathrm{p}) \sin(ut_\mathrm{d}) \exp[-\alpha(z_\mathrm{p} + z_\mathrm{d})] \times \sin(ud\cos\Theta)\sin(vd\sin\Theta) R(\alpha)\,\mathrm{d}u\,\mathrm{d}v, \quad (42)$$

which, as required, is zero for the high-symmetry case of System V ($\Theta = 0$ or $\Theta = 90^\circ$). For parallel tangent coils, $\chi = 0$, and the appropriate expression (34) is recovered from equation (41).

*2.5.1. Dipole approximation.* Expanding the integrand in equation (41) to first order in coil radius and thickness, and changing to cylindrical coordinates as before, the change in mutual impedance becomes

$$\Delta Z_{12} = \frac{\mathrm{i}\omega\mu_0 m_\mathrm{d} m_\mathrm{p}}{4\pi}\int_0^\infty \alpha^2 \exp[-\alpha(z_\mathrm{p}+z_\mathrm{d})]R(\alpha)F_3(\alpha)\,\mathrm{d}\alpha, \tag{43}$$

where, after some trigonometric manipulation, it can be shown that

$$\begin{aligned} F_3(\alpha) &= \frac{1}{2\pi}\int_0^{2\pi} \cos\varphi\cos(\varphi-\chi)\exp[\mathrm{i}\alpha d\cos(\varphi-\Theta)]\mathrm{d}\varphi \\ &= \cos\Theta\cos(\Theta-\chi)J_0(\alpha d) - \frac{\cos(2\Theta-\chi)J_1(\alpha d)}{\alpha d} \end{aligned} \tag{44}$$

and, as required, $F_3$ reduces to equation (36) in the case of parallel tangent coils, $\chi = 0$.

## 3. Experiment

The validity of the theoretical results presented in section 2 was tested by measuring the mutual impedance of a pair of well-characterized air-cored coils above a conducting plate. The two coils were similar in dimensions and were constructed by layer-winding 7 strand/41 gauge Cu 'litz' wire on an acetyl copolymer former: the coil parameters are given in table 1. The measurements were performed using two aluminium-alloy plates: the plate parameters are given in table 2. The plate dimensions were large compared with the coil dimensions and coil separation in order to minimize edge effects.

The mutual impedance was measured as a function of frequency for the various coil orientations using an HP4194a impedance/gain-phase analyzer operating in gain-phase mode. The magnitude and phase of the mutual impedance was deduced from measurements of the magnitude and phase of the ratio $v$ of the voltage $V_\mathrm{TEST}$ developed across the pickup coil and the voltage $V_\mathrm{REF}$ across a standard resistor $R_\mathrm{REF}$ inserted in series with the driver coil to monitor the driver coil current. The gain-phase analyser was interfaced to a personal computer via a GPIB card and the data acquisition was carried out using custom National Instruments LabVIEW™ virtual instrumentation software.

**Table 1.** Coil parameters.

| | Driver coil | Pickup coil |
|---|---|---|
| Inner radius | $a_{1\mathrm{d}} = 7.04\,\mathrm{mm}$ | $a_{1\mathrm{p}} = 7.04\,\mathrm{mm}$ |
| Outer radius | $a_{2\mathrm{d}} = 12.40\,\mathrm{mm}$ | $a_{2\mathrm{p}} = 12.20\,\mathrm{mm}$ |
| Thickness | $h_{3\mathrm{d}} = 2t_\mathrm{d} = 5.04\,\mathrm{mm}$ | $h_{3p} = 2t_\mathrm{p} = 5.04\,\mathrm{mm}$ |
| Number of turns | $N_\mathrm{d} = 556$ | $N_\mathrm{p} = 544$ |
| Pancake coil: liftoff | $h_{1\mathrm{d}} = 2.00\,\mathrm{mm}$ | $h_{1\mathrm{p}} = 1.98\,\mathrm{mm}$ |
| Pancake coil: centre height | $z_\mathrm{d} = 4.52\,\mathrm{mm}$ | $z_\mathrm{p} = 4.50\,\mathrm{mm}$ |
| Tangent coil: centre height | $z_\mathrm{d} = 14.0\,\mathrm{mm}$ | $z_\mathrm{p} = 14.0\,\mathrm{mm}$ |
| Isolated coil inductance (experiment) | $L_{0\mathrm{d}} = 5.84\,\mathrm{mH}$ | $L_{0\mathrm{p}} = 5.55\,\mathrm{mH}$ |
| Dc Resistance | $R_{0\mathrm{d}} = 81\,\Omega$ | $R_{0\mathrm{p}} = 52\,\Omega$ |
| Free-space resonant frequency | $f_\mathrm{Rd} = 850\,\mathrm{kHz}$ | $f_\mathrm{Rp} = 892\,\mathrm{kHz}$ |

**Table 2.** Aluminium-alloy plate parameters.

| | Plate P1 | Plate P2 |
|---|---|---|
| Thickness | $c = 5.07\,\mathrm{mm}$ | $c = 2.47\,\mathrm{mm}$ |
| Electrical resistivity | $\rho = 6.05\,\mu\Omega\,\mathrm{cm}$ | $\rho = 3.40\,\mu\Omega\,\mathrm{cm}$ |
| Magnetic permeability | $\mu_\mathrm{r} = 1.00$ | $\mu_\mathrm{r} = 1.00$ |
| Lateral dimensions | $360 \times 190\,\mathrm{mm}^2$ | $290 \times 400\,\mathrm{mm}^2$ |

The measuring circuit is shown schematically in figure 8, where $V_0$ is the driving voltage, $R_0$ is the driver-circuit series resistance, $C_0$ is the driver-circuit shunt capacitance, $R_{0\mathrm{d}}$ is the driver coil dc resistance, $Z_\mathrm{d}$ is the driver coil impedance, $M$ is the driver–pickup mutual inductance, $C_1$ is the pickup circuit shunt capacitance, $R_{0\mathrm{p}}$ is the pickup coil dc resistance, $Z_\mathrm{p}$ is the driver coil impedance and $R_1$ is the input resistance of the test channel. Following a straightforward analysis of the circuit, it can be shown that the ratio of the voltages in the test and reference channels is given by the expression

$$v = \frac{V_\mathrm{TEST}}{V_\mathrm{REF}} = \frac{\mathrm{i}\omega M}{R_\mathrm{REF}}\frac{1}{1+(R_{0\mathrm{p}}+Z_\mathrm{p})(1/R_1+\mathrm{i}\omega C_1)}. \tag{45}$$

If the input resistance $R_1$ of the measurement circuit is large, equation (45) simplifies to $v = \mathrm{i}\omega M/R_\mathrm{REF}$ and the real and imaginary parts of the mutual impedance $Z_{12} = \mathrm{i}\omega M$ are given in terms of the magnitude $|v|$ and phase $\theta$ by

$$\begin{aligned} \mathrm{Re}\,Z_{12} &= R_\mathrm{REF}|v|\cos\theta, \\ \mathrm{Im}\,Z_{12} &= R_\mathrm{REF}|v|\sin\theta \end{aligned} \tag{46}$$

and the real and imaginary parts of $M$ by

$$\begin{aligned} \mathrm{Re}\,M &= \frac{R_\mathrm{REF}\,|v|}{\omega}\sin\theta, \\ \mathrm{Im}\,M &= -\frac{R_\mathrm{REF}|v|}{\omega}\cos\theta. \end{aligned} \tag{47}$$

For the coil parameters given in table 1, together with the values $R_\mathrm{REF}$ of 18.3 Ω, shunt capacitances $C_0 = C_1$ of 28 pF and an input impedance of 1 MΩ for the reference and test channels of the HP4194a, the systematic error introduced by use of equations (46) and (47) is estimated to be less than 1% for frequencies up to 50 kHz, which was taken as the upper frequency limit for the measurements. The lower frequency limit of the measurements was largely dictated by

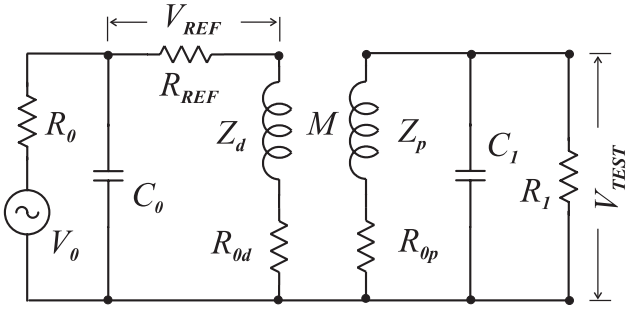


**Figure 8.** Simplified circuit illustrating the measurement of the driver–pickup coil mutual impedance.

the sensitivity of the gain-phase analyser and a lower frequency limit of 100 Hz was adopted.

In eddy-current NDI it is usual to normalize the response for single probe-coils to the isolated coil reactance $X_0 = \omega L_0$. There does not appear to be a similar convention for normalizing the transfer impedance in driver–pickup coil systems. Normalization to the isolated coil transfer reactance $\omega M_0$ suffers from the limitation that the normalizing function depends on coil separation. A more serious drawback is that this choice for the normalizing function may be zero for some configurations. Another option is to normalize the mutual impedance with respect to the geometric mean of the individual isolated coil reactance values. This normalization has the advantage of being independent of coil separation, and can be related back to the commonly used 'coupling coefficient' $k^2 = M^2/(L_{0\mathrm{d}} L_{0\mathrm{p}})$ for mutual inductance. However, in the absence of a suitable convention, we choose to present the results in terms of the change in mutual inductance due to the plate $\Delta M = \Delta Z_{12}/(\mathrm{i}\omega)$, defined as the difference in mutual inductance measured when the coils are above the plate and when same coil system is in air (i.e. isolated by a large distance from any conductors). Defined in this way, $\Delta M$ has real and imaginary parts, and scales with frequency in the same way as the other candidates for a normalized transfer impedance.

## 4. Results

The change in mutual inductance due to the plate P1 was measured as a function of frequency for the four high-symmetry coil configurations (Systems I–IV). The coil separation for each case is given in table 3 and corresponds to the smallest achievable separation for each configuration while maintaining the minimum coil liftoff (coil centre height). The results are shown for the pancake coil configuration System I in figure 9, the pancake–tangent coil configuration System II in figure 10 and for the parallel tangent coil configurations Systems III and IV in figures 11 and 12. The results of the theoretical calculations, obtained by numerical integration of the exact closed-form expressions derived in section 2, are also shown. The experimental results are in excellent agreement with the theoretical calculations. The small deviations observed at very high frequencies are due to non-ideal coil behaviour arising from stray capacitance. There are no free parameters in the calculations.

For these coil separations, the variation in $\Delta M$ with frequency is similar for the three configurations involving a tangent coil orientation. In these cases, the imaginary part of $\Delta M$ exhibits a minimum in the vicinity of 200–400 Hz and the real part varies monotonically, tending to a constant value at high frequency. The variation of $\Delta M$ with frequency for the pancake coil configuration is qualitatively different; both the real and imaginary parts of $\Delta M$ have zero crossings in the range 100 Hz–1 kHz with the imaginary part tending to zero and real part tending to a constant value at high frequency.

The dependence of $\Delta M$ on coil separation at constant frequency was also investigated for the high-symmetry configurations Systems I–IV. Illustrative results for the pancake coil geometry (System I) are shown in figure 13 for pancake coils on the larger plate P2 at a frequency of 200 Hz. The experimental results are again in excellent agreement with the theoretical predictions using the exact result equation (17). The predicted variation using the dipole approximation (20) is also shown in figure 13. As expected, the dipole approximation is in reasonable agreement with both the experimental results and the exact theory for large coil separation but becomes increasingly inaccurate as the coil separation is reduced.

## 5. Discussion

A series of closed-form expressions for $\Delta Z_{12}$ was derived in section 2 for all possible configurations of cylindrical air-cored coils in which the orientation of the individual coils is either tangential or normal to the surface of the plate. These results allow the effects of coil geometry, liftoff, conductivity variation and variation in plate thickness to be calculated using straightforward numerical integration routines. The validity of the analysis is established by the excellent agreement between theoretical predictions and the experimental results in four high-symmetry cases. The general expressions also reduce to the correct form in the dipole limit, providing further confidence in the results.

This work also confirms that expressions for $\Delta Z_{12}$ obtained in the dipole limit, while useful in the geophysics context where the coil separation is large, are inadequate for accurate calculations in eddy-current NDI where the source and receiver coils are typically in close proximity. In these cases, the exact theory should be used. The dipole approximation is valuable in qualitative studies because of its relative simplicity in most cases.

The central result (9) for $\Delta Z_{12}$ due to eddy-current induction is valid for air-cored coils with arbitrary shape. The application to other-than-circular coil geometries is straightforward if the appropriate (free-space) source functions defined by equation (10) for the driver and pickup coils are known. Source functions for rectangular coils with rectangular cross-section oriented parallel or perpendicular to the surface of the plate can be deduced from known expressions for the free-space second-order vector potential (Theodoulidis and Kriezis 2002) so that a systematic study of rectangular driver–pickup coils could be readily attempted. For air-cored coils with general shape, analytical expressions for the source field can be derived in principle using the Biot–Savart law.

**Table 3.** Driver–pickup coil parameters: the individual coil parameters (liftoff, centre height, etc) are given in table 1.

| | System I | System II | System III | System IV |
|---|---|---|---|---|
| Driver coil orientation | Pancake | Pancake | Tangent | Tangent |
| Pickup coil orientation | Pancake | Tangent | Tangent | Tangent |
| Separation, $d$ | 28.0 mm | 18.5 mm | 9.0 mm | 28.0 mm |
| Mutual Inductance in air, $M_0$ | $-171.5\,\mu$H | $318.5\,\mu$H | 1.62 mH | $-171.5\,\mu$H |

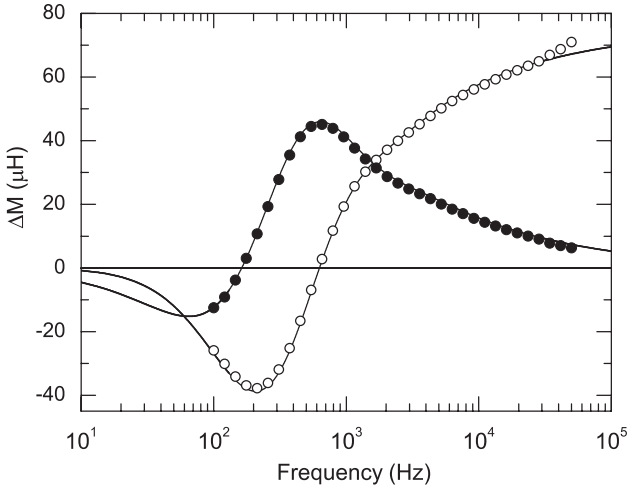


**Figure 9.** Change in mutual inductance due to the Al-alloy plate P1 as a function of frequency for the pancake coil geometry (System I). The calculated variation according to equation (17) is shown by the solid curves. The measured values are denoted by the symbols: real part (○), imaginary part (●).

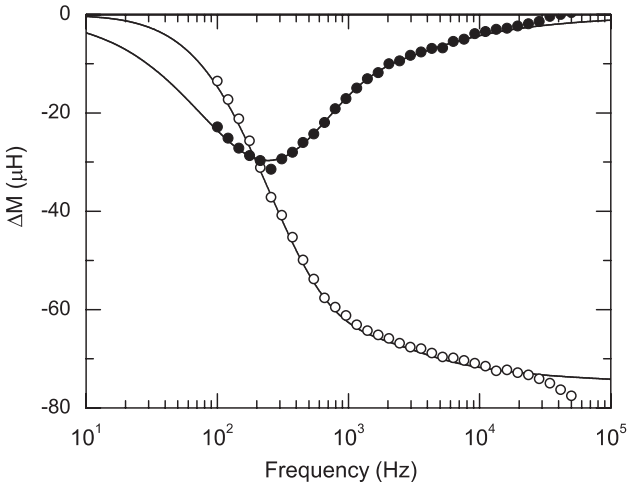


**Figure 11.** Change in mutual inductance due to the Al-alloy plate P1 as a function of frequency for the parallel tangent coil geometry with $\Theta = 0$ (System III). The calculated variation according to equation (34) is shown by the solid curves. The measured values are denoted by the symbols: real part (○), imaginary part (●).

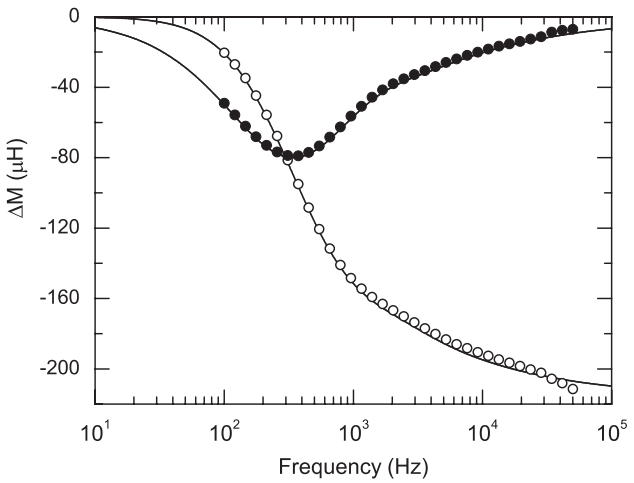


**Figure 10.** Change in mutual inductance due to the Al-alloy plate P1 as a function of frequency for the pancake–tangent coil geometry with $\Theta = 0$ (System II). The calculated variation according to equation (26) is shown by the solid curves. The measured values are denoted by the symbols: real part (○), imaginary part (●).

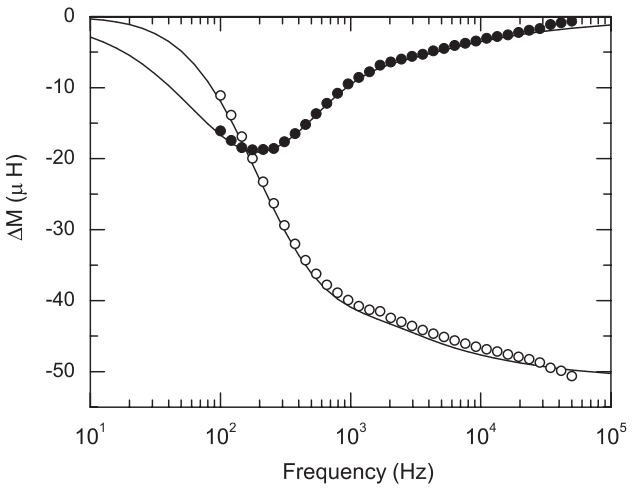


**Figure 12.** Change in mutual inductance due to the Al-alloy plate P1 as a function of frequency for the parallel tangent coil geometry with $\Theta = 90^\circ$ (System IV). The calculated variation according to equation (34) is shown by the solid curves. The measured values are denoted by the symbols: real part (○), imaginary part (●).

However, for highly complex coil geometries, the resulting expressions may be overly cumbersome and an alternative approach may be more effective (e.g. finite-element analysis). Irrespective of the detailed coil geometry, the expressions for $\Delta M$ must reduce to the appropriate dipole expression (section 2) in the limit of small coil dimensions.

The analysis can be extended to more complicated layered systems by replacing the reflection coefficient $R(\alpha)$ given by equation (7) for a conducting plate by the appropriate reflection coefficient for a layered half-space. For example, $\Delta M$ due to a conducting coating on a thick metal substrate can be calculated for the coil systems in sections 2.2–2.5 by employing the known reflection coefficient for a two-layer half-space (Dodd and Deeds 1968). The extension to a plate with horizontal uniaxial anisotropy also appears relatively straightforward and would involve the replacement of the isotropic reflection coefficient with the anisotropic reflection coefficient $R(u, v)$, given, for example, by Burke (1990). The present theory was tested using non-magnetic plates ($\mu_r = 1$) but is also expected to be valid for paramagnetic and ferromagnetic plates ($\mu_r > 1$) provided the magnetic properties can be approximated by an effective linear permeability.

While the response to crack-like defects is not treated in this paper, all six of the canonical coil configurations can be used for defect detection. The pancake coil geometry (System I) is perhaps the most widely used in practice. As all the configurations are 'geometrically anisotropic' they are well suited to detection of directional defects, such as fatigue cracks (Mayos and Muller 1987). Coil configurations such as Systems V and VI, for which $\Delta Z_{12} = 0$ irrespective

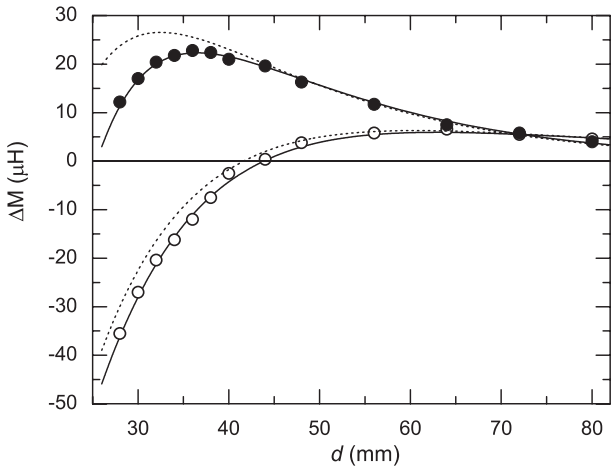


**Figure 13.** Change in mutual inductance due to the Al-alloy plate P2 as a function of coil separation $d$ for the pancake coil geometry (System I) at 200 Hz. The calculated variation equation (17) is shown by the solid curves and the dipole approximation equation (20) by the dotted curves. The measured values are denoted by the symbols: real part (○), imaginary part (●).

of frequency, separation and liftoff, are significant because any change in mutual impedance must, in principle, be due to the presence of a defect. The only qualification is that the coil configuration must remain unchanged during the inspection, i.e. there is no tilt or misalignment. For other coil configurations, $\Delta Z_{12}$ is zero for a particular separation (e.g. System II $d = 0$) or the real and imaginary parts are separately zero for particular combinations of frequency and separation (Systems I, III, IV), which may also provide advantages in defect detection. Further work is required to develop explicit models for $\Delta Z_{12}$ due to cracks, hidden corrosion or other discontinuities. Such models, combined with the results presented here for a defect-free plate, would provide a useful starting point for optimizing inspection parameters in eddy-current NDI.

In practical eddy-current testing, the pickup coil voltage alone is usually measured rather than the ratio of the pickup coil voltage to the driver coil current (Dodd *et al* 1979, Dodd and Deeds 1982). Hence, to predict the change in pickup coil voltage, it is also necessary to know a number of additional circuit parameters: notably, the mutual inductance of the coils in air $M_0$, the self-impedance of the driver coil $Z_d$ and the self-impedance of the pickup coil $Z_p$. The self-impedance values are the sum of the respective free-space coil impedance and the change in coil self-impedance due to eddy-current induction in the plate. For circular air-cored coils above a conducting plate, the self-inductance can be calculated using well-established closed-form expressions for the pancake coil geometry (Dodd and Deeds 1968) and the tangent coil geometry (Burke 1986, Clark and Bond 1990). Similarly, the mutual inductance of circular air-cored coils in free-space can be calculated using established formulae (Grover 1946).

## Acknowledgments

The authors are grateful to Prof. Peter Wells (Monash University) and Dr Robert Ditchburn (DSTO) for helpful discussions. MEI wishes to acknowledge the support of the Department of Defence Studybank Scheme.

© Commonwealth of Australia

## Appendix

From equation (6), the two-dimensional Fourier transform of the function

$$F(x, y) = \int_0^\infty g(s) J_0\big[s\sqrt{(x - x_0)^2 + (y - y_0)^2}\big]\,\mathrm{d}s, \qquad \text{(A1)}$$

is defined as

$$\tilde{F}(u, v) = \frac{1}{2\pi}\int_{-\infty}^{\infty} \mathrm{d}x \exp(-\mathrm{i}ux)\int_{-\infty}^{\infty} \mathrm{d}y \exp(-\mathrm{i}vy) \times \int_0^\infty \mathrm{d}s\, g(s) J_0\big[s\sqrt{(x - x_0)^2 + (y - y_0)^2}\big].$$

Changing variables so that $x' = x - x_0$ and $y' = y - y_0$

$$\tilde{F}(u, v) = \frac{1}{2\pi}\exp(-\mathrm{i}ux_0 - \mathrm{i}vy_0)\int_{-\infty}^{\infty} \mathrm{d}x' \exp(-\mathrm{i}ux') \times \int_{-\infty}^{\infty} \mathrm{d}y' \exp(-\mathrm{i}vy')\int_0^\infty \mathrm{d}s\, g(s) J_0(s\rho')$$

and converting to a cylindrical polar coordinate system with $\rho' = \sqrt{(x')^2 + (y')^2}$

$$\tilde{F}(u, v) = \exp(-\mathrm{i}ux_0 - \mathrm{i}vy_0)\int_0^\infty \mathrm{d}\rho' \rho' J_0(\alpha\rho') \times \int_0^\infty \mathrm{d}s\, g(s) J_0(s\rho'), \qquad \text{(A2)}$$

where $\alpha^2 = u^2 + v^2$. Equation (A2) can then be evaluated using the Fourier–Bessel theorem to yield the final result

$$\tilde{F}(u, v) = \frac{\exp(-\mathrm{i}ux_0 - \mathrm{i}vy_0) g(\alpha)}{\alpha}. \qquad \text{(A3)}$$

Consider next the Fourier transform of a function of the form

$$G(x, y) = \int_0^\infty \int_0^\infty f(s) m(q) \sin[s(x - x_0)] \times \cos[p(y - y_0)]\,\mathrm{d}s\,\mathrm{d}p, \qquad \text{(A4)}$$

where $f(s)$ is assumed to be an odd function of $s$ and $q^2 = p^2 + s^2$. The Fourier transform is thus

$$\tilde{G}(u, v) = \frac{1}{2\pi}\int_{-\infty}^{\infty}\int_{-\infty}^{\infty} \mathrm{d}x\,\mathrm{d}y \exp(-\mathrm{i}ux - \mathrm{i}vy) \times \int_0^\infty\int_0^\infty \mathrm{d}s\,\mathrm{d}p\, f(s) m(q) \sin[s(x - x_0)] \cos[p(y - y_0)].$$

Changing variables so that $x' = x - x_0$ and $y' = y - y_0$ and interchanging the order of integration,

$$\tilde{G}(u, v) = \frac{1}{2\pi}\exp(-\mathrm{i}ux_0 - \mathrm{i}vy_0)\int_0^\infty\int_0^\infty \mathrm{d}s\,\mathrm{d}p\, f(s) m(q) \times \int_{-\infty}^{\infty}\int_{-\infty}^{\infty} \mathrm{d}x'\,\mathrm{d}y' \exp(-\mathrm{i}ux' - \mathrm{i}vy') \sin(sx') \cos(py').$$

Hence, using the orthogonality properties of the trigonometric functions together with the odd symmetry of $f(s)$,

$$\tilde{G}(u, v) = -\frac{\mathrm{i}\pi}{2}\exp(-\mathrm{i}ux_0 - \mathrm{i}vy_0) f(u) m(\alpha). \qquad \text{(A5)}$$

## References


Auld B A and Moulder J C 1999 *J. Nondestr. Eval.* **18** 3–36

Auld B A, Moulder J C, Jefferies S, Schull P J, Ayter S and Kennedy J 1989 *Res. Nondestr. Eval.* **1** 1–11

Beissner R E 1988 *J. Nondestr. Eval.* **7** 25–34

Beissner R E and Sablik M J 1984 Theory of electric current perturbation probe optimisation *Review of Progress in Quantitative NDE* vol 3A, ed D O Thompson and D E Chimenti (New York: Plenum) pp 633–41

Burke S K 1986 *J. Phys. D: Appl. Phys.* **19** 1159–73

Burke S K 1990 *J. Appl. Phys.* **68** 3080–90

Clark R and Bond L J 1990 *IEE Proc.* A **137** 141–6

Cecco V S, Carter J S and Sullivan S P 1993 *Mater. Eval.* **51** 572–7

Deeds W E, Dodd C V and Scott G W 1979 Computer-aided design of multi-frequency eddy-current tests for layered conductors with multiple property variations *Internal Report* ORNL/TM-6858 Oak Ridge National Laboratory, USA

Dodd C V, Cheng C C and Deeds W E 1974 *J. Appl. Phys.* **45** 638–47

Dodd C V and Deeds W E 1968 *J. Appl. Phys.* **39** 2829–38

Dodd C V and Deeds W E 1982 Absolute eddy-current measurements of electrical conductivity *Review of Progress in Quantitative NDE* vol 1, ed D O Thompson and D E Chimenti (New York: Plenum) pp 387–93

Dodd C V, Deeds W E and Luquire J W 1971 Integral solutions to some eddy-current problems *Physics and Nondestructive Testing* vol 2, ed W J McGonnagle (London: Gordon and Breach) pp 233–93

Grimberg R, Savin A, Radu E and Mihalache O 2000 *IEEE Trans. Magn.* **36** 299–307

Grover F W1946 *Inductance Calculations, Working Formulas and Tables* (New York: Van Nostrand)

Hannakam L 1972 *Arch. Elektrotech.* **54** 215–61

Haugland S M 1996 *IEEE. Trans. Magn.* **32** 3195–211

Hoshikawa H, Koyama K and Karasawa H 2001 A new ECT surface probe without liftoff noise and with phase information on flaw depth *Review of Progress in Quantitative NDE* vol 20, ed D O Thompson and D E Chimenti (Melville, NY: American Institute of Physics) CP557, pp 969–76

Mayos M and Muller J L 1987 *J. Nondestr. Eval.* **6** 109–16

Obrutsky L S, Cecco V S, Sullivan S P and Humphrey D 1996 *Mater. Eval.* **54** 93–8

Popa R C, Miya K and Kurokawa M 1997 *J. Nondestr. Eval.* **16** 161–73

Schmidt T R 1989 *Mater. Eval.* **47** 14–22

Theodoulidis T P and Kriezis E E 2002 *NDT&E Int.* **35** 407–14

Wait J R 1982 *Geo-electromagnetism* (London: Academic) pp 121–6

Zhang Z, Routh P S, Oldenburg D W, Alumbaugh D L and Newman G A 2000 *Geophys.* **65** 492–501